

Orientation determination of nitrogen-vacancy center in diamond using a static magnetic field

Yangpeng Wang(王杨鹏), Rujian Zhang(章如健), Yan Yang(杨燕), Qin Wu(吴琴), Zhifei Yu(于志飞)‡, and Bing Chen(陈冰)

Citation: Chin. Phys. B, 2023, 32 (**7**): 070301. DOI: 10.1088/1674-1056/acc0f7
Journal homepage: http://cpb.iphy.ac.cn; http://iopscience.iop.org/cpb

What follows is a list of articles you may be interested in

High-fidelity quantum sensing of magnon excitations with a single electron spin in quantum dots

Le-Tian Zhu(朱乐天), Tao Tu(涂涛), Ao-Lin Guo(郭奥林), and Chuan-Feng Li(李传锋)
Chin. Phys. B, 2022, 31 (**12**): 120302. DOI: 10.1088/1674-1056/ac8919

Optical scheme to demonstrate state-independent quantum contextuality

Ya-Ping He(何亚平), Deng-Ke Qu(曲登科), Lei Xiao(肖磊), Kun-Kun Wang(王坤坤), and Xiang Zhan(詹翔)
Chin. Phys. B, 2022, 31 (**3**): 030305. DOI: 10.1088/1674-1056/ac229f

Quantum information processing with nitrogen-vacancy centers in diamond

Gang-Qin Liu(刘刚钦), Xin-Yu Pan(潘新宇)
Chin. Phys. B, 2018, 27 (**2**): 020304. DOI: 10.1088/1674-1056/27/2/020304

Time-bin-encoding-based remote states generation of nitrogen-vacancy centers through noisy channels

Su Shi-Lei (苏石磊), Chen Li (陈丽), Guo Qi (郭奇), Wang Hong-Fu (王洪福), Zhu Ai-Dong (朱爱东), Zhang Shou (张寿)
Chin. Phys. B, 2015, 24 (**2**): 020305. DOI: 10.1088/1674-1056/24/2/020305

Quantum Fisher information and spin squeezing in one-axis twisting model

Zhong Wei (钟伟), Liu Jing (刘京), Ma Jian (马健), Wang Xiao-Guang (王晓光)
Chin. Phys. B, 2014, 23 (**6**): 060302. DOI: 10.1088/1674-1056/23/6/060302

Orientation determination of nitrogen-vacancy center in diamond using a static magnetic field

Yangpeng Wang(王杨鹏)[†], Rujian Zhang(章如健)[†], Yan Yang(杨燕), Qin Wu(吴琴), Zhifei Yu(于志飞)[‡], and Bing Chen(陈冰)[§]

Department of Physics, Hefei University of Technology, Hefei 230009, *China*

(Received 28 December 2022; revised manuscript received 13 January 2023; accepted manuscript online 3 March 2023)

Nitrogen-vacancy (NV) centers in a bulk diamond are often employed to realize measurement of multiple physical quantities, which depends on orientation information of NV axis. We report a fast and effective method to determine the orientation of NV axis with the aid of a static magnetic field. By measuring the optically detected magnetic resonance spectra, we can precisely extract the polar angle information between the NV axis and the known magnetic field. Combining with the polar angle information of different kinds of NV centers, we employ the Nelder–Mead algorithm to get the optimal solution of the orientation of NV axis. This method is simple and efficient, and is easily applied in NV-based quantum sensing.

Keywords: nitrogen-vacancy centers, polar angle, quantum sensing

PACS: 03.65.Ta, 42.50.Ct, 61.72.jn, 76.70.Hb **DOI:** 10.1088/1674-1056/acc0f7

1. Introduction

Nitrogen-vacancy (NV) center particularly in the negative charge state in diamond is a promising solid-state system for quantum information processing and quantum sensing,[1–7] which can be initialized and detected by optical pumping.[6,8,9] The electron spin of NV center has long coherence time under ambient conditions.[10] Its electron spin state information can be easily extracted by optically detected magnetic resonance (ODMR) spectra.[9] Its electron spin is sensitive to multiple physical quantities, which makes it possible to be a promising quantum sensor for multiple physical quantities with high sensitivity and spatial resolution, such as electric field,[11,12] magnetic field,[13–16] temperature,[17,18] and crystal strain.[19,20] Accurate and reliable measurement of NV orientation is a crucial step when one attempts to utilize the NV centers for solid-state quantum sensing.

For a single crystal sample, the orientation of the NV axis has four possibilities with knowledge of the crystalline facet in diamond.[21] However, NV centers are randomly distributed in diamond, and their positions and orientations are difficult to identify in the laboratory frame. Therefore, it is necessary to develop a fast and effective method to identify NV orientation for further potential applications. A traditional method to identify NV orientation is to measure ODMR spectra with a series of three-dimensional magnetic fields parallel to the X–Y plane and along the Z axis.[22] Takashima *et al.*[23] proposed an improved method that can reduce the measurement time by half. The improved method only needs to measure a single dataset of ODMR spectra by rotating the magnetic field in X–Y plane and a group ODMR spectra of magnetic field in a single direction out of X–Y plane. These methods are still time-consuming due to measuring plentiful ODMR spectra. For the NV ensembles experiment, the coordinates (X, Y, Z) often consist of X, Y, and Z axes that are often considered to be along [110], [$\bar{1}$10], and [001] in terms of diamond lattice vectors, respectively.[24] Therefore, the actual orientations of NV axis are still unclear in real space. It is essential to develop a fast and effective method to determine the orientation of the NV axis for quantum sensing based on NV ensembles and single spins in single crystal sample.

In this work, we propose a fast and effective method to simultaneously identify the orientation of four different NV axes assisted with a direction-known magnetic field in the laboratory frame. We just need to measure the ODMR spectra of three different kinds of NV centers and then employ the Nelder–Mead algorithm to calculate the orientation information of NV axis in bulk diamond. Polar angle θ and azimuthal angle ϕ are used to describe the orientation of NV axis in the laboratory frame. A direction-known magnetic field with vector orientation $(\theta_{\rm B},\ \phi_{\rm B}) = (50.29^\circ, 78.75^\circ)$ is used in the experiment. We finally calculate that the orientation information of four different NV axes is $(\theta_{\rm NV0},\ \phi_{\rm NV0}) = (2.03 \pm 0.20^\circ, 287.48 \pm 23.04^\circ)$, $(\theta_{\rm NV1},\ \phi_{\rm NV1}) = (110.81 \pm 0.48^\circ, 331.57 \pm 0.44^\circ)$, $(\theta_{\rm NV2},\ \phi_{\rm NV2}) = (107.69 \pm 0.27^\circ, 91.30 \pm 0.80^\circ)$ and $(\theta_{\rm NV3},\ \phi_{\rm NV3}) = (109.97 \pm 0.84^\circ, 210.54 \pm 0.42^\circ)$, respectively. In our approach, owing to only measuring three different kinds of ODMR spectra, the measurement time can be greatly reduced.

[†]These authors contributed equally to this paper.

[‡]Corresponding author. E-mail: zfyu-phy@hfut.edu.cn

[§]Corresponding author. E-mail: bingchenphysics@hfut.edu.cn

© 2023 Chinese Physical Society and IOP Publishing Ltd

In the experiment, ODMR spectra of NV_1, NV_2, and NV_3 centers are used to realize the identification of NV orientations, and ODMR spectra of NV_0 center is employed to verify the experimental results. By comparing the theoretical and experimental results of NV_0's ODMR resonance line, there are deviations of 1.16 MHz and 1.01 MHz with errors of 1.71% and 1.48%, respectively, for left and right resonance peaks of NV_0 center in the results, which means that our method is effective and accurate.

2. Results and discussion

2.1. Basic properties

The diamond lattice consists of covalently bond carbon atoms that are tetrahedrally bonded to each other through sp^3 hybrid bonds (distance 1.44 Å) with bond angle of 109.47°. The NV center in diamond is a point defect and consists of a substitutional nitrogen atom and an adjacent vacancy at the diamond lattice as shown in Fig. 1(a). In the diamond lattice, there are four kinds of NV centers with different tetrahedral orientations referring to the laboratory frame due to the C_{3v} symmetry.

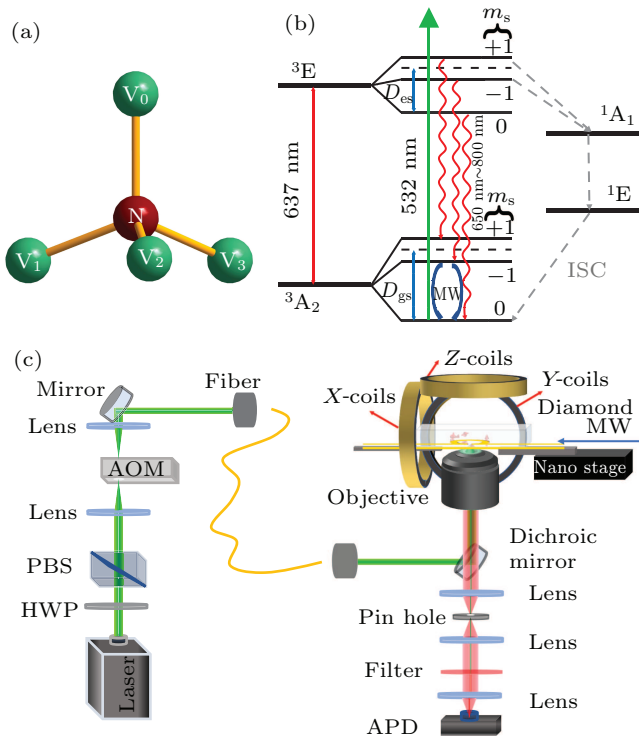


Fig. 1. (a) Schematics of the NV center in diamond. NV_0, NV_1, NV_2, NV_3 represent tetrahedral orientations for four kinds of NV centers referring to the laboratory frame. (b) Energy-level scheme of the NV center in diamond. The ground state ($^3A_2$) and excited state (^3E) of NV center are both spin triplets, whose zero-splittings are $D_{gs} = 2.87$ GHz and $D_{es} = 1.43$ GHz, respectively. Due to the Zeeman effect, the resonance lines between $m_s = 0$ and $m_s = \pm 1$ in $^3A_2$ (^3E) are separated around 2.87(1.43) GHz in an applied magnetic field. (c) Schematics of the experimental setup with a home-built confocal microscopy. The Gaussian beam is focused on the diamond and the fluorescence photons are collected by oil-immersion microscope objective. MW: microwave, HWP: half wave plate, PBS: polarization beam splitter, APD: single photon avalanche diode.

The electron spin energy levels of the NV center are illustrated in Fig. 1(b). Here, 532 nm laser pulse is used to pump the NV center from the ground state $^3A_2$ to the excited state ^3E. The NV center's electron spin can decay from the excited state ^3E to the ground state $^3A_2$ by radiative transitions directly or spin-selective nonradiative inter-system crossings (ISC), which can enable optical initialization and readout of the electronic spin state. The electron spin can be manipulated by a microwave field resonant with the transitions between $m_s = 0$ and $m_s = \pm 1$ in $^3A_2$.

2.2. Experimental setup

The experiment is performed based on a purpose-built confocal microscope system as shown in Fig. 1(c), which is employed to address and focus the 532 nm laser beam to the individual NV center. The diamond sample used in the experiment is a type-IIa, single-crystal synthetic diamond (element six). We use an acousto-optic modulator (AOM) to modulate the laser beam and to produce the required laser sequences. The produced laser beam passes through the single mode optical fiber and converts to a near-Gaussian beam. The fluorescence of the NV center can be collected by an oil-immersion microscope objective with NA = 1.40 and filtered by pin hole and long pass filter. Finally, the fluorescence photons are detected by a single photon avalanche diode (APD).

2.3. Theoretical analysis

Under external magnetic field conditions, the spin Hamiltonian H can be written as the sum of zero-field splitting term, electron spin Zeeman splitting term, and local strain term in the NV center. H is expressed as[25]

$$H = D_{gs}\left(S_z^2 - \frac{S(S+1)}{3}\right) + \mu_B g_e \boldsymbol{B}\cdot\boldsymbol{S} + E(S_x^2 - S_y^2), \quad (1)$$

where $D_{gs} \sim 2.87$ GHz is zero-field splitting parameter, $\boldsymbol{S} = (S_x, S_y, S_z)$ is the spin matrices of spin-1 systems, μ_B is the Bohr magneton, g_e is the g-factor of electron, $\boldsymbol{B}$ is the external magnetic field and $E \sim 0$ is the strain splitting due to imperfect axial symmetry. Considering that magnetic field $\boldsymbol{B}$ has transverse $\boldsymbol{B}_\perp$ [$\boldsymbol{B}_\perp = (B_x, B_y)$] and axial $\boldsymbol{B}_z$ components, and the strain splitting is approximately equal to zero in single-crystal synthetic bulk diamond. The spin Hamiltonian can be written as[25]

$$H = \begin{pmatrix} \frac{D}{3} - \mu_B g_e B_z & -\mu_B g_e \frac{B_x - iB_y}{\sqrt{2}} & 0 \\ -\mu_B g_e \frac{B_x + iB_y}{\sqrt{2}} & -\frac{2D}{3} & -\mu_B g_e \frac{B_x - iB_y}{\sqrt{2}} \\ 0 & -\mu_B g_e \frac{B_x + iB_y}{\sqrt{2}} & \frac{D}{3} + \mu_B g_e B_z \end{pmatrix}, \quad (2)$$

and $m_s = 0$, $m_s = -1$, $m_s = +1$ are the eigenvalues. The spin transition frequencies of $m_s = 0 \to m_s = -1$ and $m_s = 0 \to m_s = +1$ are defined as ν_1 and ν_2. The transition frequencies

are given to the third order in $\frac{\mu_B g_e B}{hD_{gs}}$ by[26]

$$\nu_1 = D_{gs}\left[1-\left(\frac{\mu_B g_e B}{hD_{gs}}\right)\cos\alpha+\frac{3}{2}\left(\frac{\mu_B g_e B}{hD_{gs}}\right)^2\sin^2\alpha - \left(\frac{\mu_B g_e B}{hD_{gs}}\right)^3\left(\frac{1}{8}\sin^3\alpha\tan\alpha-\frac{1}{2}\sin^2\alpha\cos\alpha\right)\right], \quad (3)$$

$$\nu_2 = D_{gs}\left[1+\left(\frac{\mu_B g_e B}{hD_{gs}}\right)\cos\alpha+\frac{3}{2}\left(\frac{\mu_B g_e B}{hD_{gs}}\right)^2\sin^2\alpha + \left(\frac{\mu_B g_e B}{hD_{gs}}\right)^3\left(\frac{1}{8}\sin^3\alpha\tan\alpha-\frac{1}{2}\sin^2\alpha\cos\alpha\right)\right], \quad (4)$$

where h is the Planck constant, and α is the angle between the magnetic field and the NV axis.

In experiment, we measure the ODMR spectra and obtain the transition frequencies ν_1 and ν_2 by fitting resonant peaks with the Lorentzian function. The angle α between the magnetic field and the NV axis can be obtained by solving Eqs. (3) and (4). However, it is not enough to identify the orientation of NV axis because the angle α only tells us that the possible NV orientation is a cone around the magnetic field as depicted in Fig. 2(c).

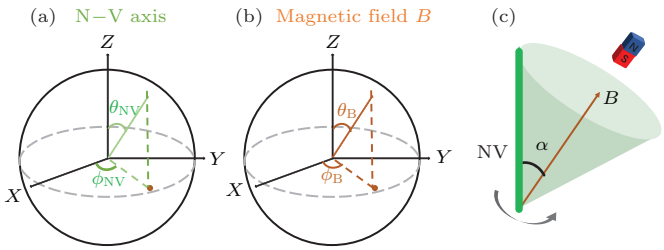


Fig. 2. (a) and (b) Orientation of the NV axis $\mathrm{NV_i} = (\theta_{\mathrm{NVi}},\ \phi_{\mathrm{NVi}})$ $(i = 1,2,3,4)$ and the orientation of the magnetic field $\boldsymbol{B} = (\theta_B,\ \phi_B)$. The brown arrow indicates the direction of the magnetic field, and the green arrow indicates the direction of the NV axis. (c) The possible direction position of NV axis corresponding to single ODMR spectra. In static magnetic field, the orientation of NV axis is possibly located at a conical surface calculated by ODMR spectra.

Here, we define the angle $(\theta_{\mathrm{NV}i},\ \phi_{\mathrm{NV}i})$ $(i = 1,\ 2,\ 3,\ 4)$ as the orientation of the NV axis and $(\theta_B,\ \phi_B)$ as the orientation of the magnetic field in the laboratory frame (spherical coordinates), as shown in Figs. 2(a) and 2(b), where the laboratory frame is transformed from the Cartesian coordinate system formed by three-dimensional coils with X-coils corresponding to X-axis, Y-coils corresponding to Y-axis, and Z-coils corresponding to Z-axis in real space. Therefore, the orientation of the NV axis can be transformed into the vector $\mathrm{NV}_i = (x_{\mathrm{NV}i}, y_{\mathrm{NV}i}, z_{\mathrm{NV}i}) = (\sin\theta_{\mathrm{NV}i}\cos\phi_{\mathrm{NV}i},\ \sin\theta_{\mathrm{NV}i}\sin\phi_{\mathrm{NV}i},\ \cos\phi_{\mathrm{NV}i})$ $(i = 1,\ 2,\ 3,\ 4)$ and $\boldsymbol{B} = (x_B, y_B, z_B) = (\sin\theta_B\cos\phi_B,\ \sin\theta_B\sin\phi_B,\ \cos\phi_B)$ in these Cartesian coordinates. In diamond lattice, the relationship between the NV axial vector and the magnetic field vector can be given as follows:

$$\mathrm{NV}_i\cdot\mathrm{NV}_j = \cos 109.47^\circ, \quad (5)$$

$$\mathrm{NV}_k\cdot\boldsymbol{B} = \cos\alpha_k, \quad (6)$$

where NV_i, NV_j $(i,j = 0,\ 1,\ 2,\ 3$ and $i \neq j)$, α_k $(k = 1,\ 2,\ 3)$ represent the angles between the NV axis ($\mathrm{NV_1}$, $\mathrm{NV_2}$, and $\mathrm{NV_3}$) and the magnetic field $\boldsymbol{B}$, as shown in Fig. 1(a)). Based on Eqs. (5) and (6), we are able to calculate the final values of the four NV orientations using the Nelder–Mead algorithm and obtain the angle α.

The Nelder–Mead algorithm is one of the best known algorithms for multidimensional unconstrained optimization without derivatives. For the n-dimensional minimization problem $\min f(x)$, with a simpler description, the method for searching the minimum value is described as follows: (i) Generate initial values x_l $(l = 2,3,\ldots,n+1)$ next to x_0 we give. (ii) Find minimum point x_m in the $f(x_l)$. (iii) Take x_m as the new initial value, and repeat steps (i) and (ii) until local minimum appears. The constraint equation is $\min f(x) = \sum_{k=1}^{3}(\mathrm{NV}_k\cdot\boldsymbol{B}-\cos(\alpha_k))^2 + \sum_{k=1}^{3}(\mathrm{NV}_k\cdot\mathrm{NV}_0-\cos(109.47^\circ))^2 + \sum_{k=2}^{3}(\mathrm{NV}_k\cdot\mathrm{NV}_1-\cos(109.47^\circ))^2 + \sum_{k=3}^{3}(\mathrm{NV}_k\cdot\mathrm{NV}_2-\cos(109.47^\circ))^2$, where α_k is the the angles between the NV axis and the magnetic field as shown in Eqs. (5) and (6), and NV_k is the results of each search. In the experiment, first the initial value with four NV axis' parameters is randomly given, considering the internal bond angle (109.47°) of diamond crystal. Because the search result of the Nelder–Mead algorithm is the local minimum, some initial values with large numerical differences are given to find the absolute minimum of the equation $\min f(x)$. Then angles of first initial value are rotated for t $(t = 30^\circ, 60^\circ, 90^\circ, 120^\circ, 150^\circ, 180^\circ)$ around the Y-axis to produce a series of new initial values by rotation matrix.[27] Later, when a series of initial values are applied, the local minimum can be searched by the Nelder–Mead algorithm. Finally, when the absolute minimum appears, the NV_k is the final search result.

2.4. Results

In the experiment, four kinds of NV centers close to each other (several microns) are selected through the difference of ODMR spectra. In the confocal microscope system the positions of laser focus and oil-immersion microscope objective are fixed. Therefore, the different NV centers in diamond can be moved to the same laser focus by nano-piezoelectric stage in order to ensure that each NV center is under the same magnetic field. Then, we sweep the microwave (MW) frequency and obtain the ODMR spectra. Compared to the continuous ODMR scheme, the pulsed ODMR scheme with a resonant MW π-pulse and a read-out laser pulse can reduce the power broadening of ODMR spectra and improve spectral resolution. At low MW power (π-pulse duration of $\sim$ 2600 ns), we can observe the hyperfine splitting in the ODMR spectra due to the hyperfine interaction between electronic spin and nitrogen

nuclear spin. Four sets of pulsed ODMR spectra are measured in a [111]-oriented bulk diamond with the certain static magnetic field as shown in Fig. 3. The transition frequencies of left peak ($m_s = 0$, $m_I = -1 \rightarrow m_s = -1$, $m_I = -1$), middle peak ($m_s = 0$, $m_I = 0 \rightarrow m_s = -1$, $m_I = 0$) and right peak ($m_s = 0$, $m_I = +1 \rightarrow m_s = -1$, $m_I = +1$) in the ground state $^3A_2$ are same. For convenience, the middle peaks (ν_1 and ν_2) are selected and correspond to the transition frequencies of $m_s = 0$, $m_I = 0 \rightarrow m_s = -1$, $m_I = 0$ and $m_s = 0$, $m_I = 0 \rightarrow m_s = +1$, $m_I = 0$, which are shown in Table 1.

Table 1. The transition frequencies for NV centers in different orientations. The angles α between the static magnetic field and the NV axis are extracted from the ODMR spectra of NV_1 center, NV_2 center, and NV_3 center as shown in Fig. 3. The last column is the final orientations of NV_i ($i = 0, 1, 2, 3$) shown in Fig. 4(b).

	NV_0	NV_1	NV_2	NV_3
ν_1	2806.54±0.16 MHz	2827.48±0.18 MHz	2818.32±0.16 MHz	2797.22±0.16 MHz
ν_2	2942.22±0.16 MHz	2923.71±0.16 MHz	2931.93±0.12 MHz	2950.27±0.16 MHz
α	–	$\alpha_1 = 116.20°$	$\alpha_2 = 58.60°$	$\alpha_3 = 134.63°$
(θ, ϕ)	$(2.03 \pm 0.20°,\ 287.48 \pm 23.04°)$	$(110.81 \pm 0.48°,\ 331.57 \pm 0.44°)$	$(107.69 \pm 0.27°,\ 91.30 \pm 0.80°)$	$(109.97 \pm 0.84°,\ 210.54 \pm 0.42°)$

According to the ODMR spectra shown in Fig. 3, the angle α between the magnetic field $\boldsymbol{B}$ and the NV axis is calculated by Eqs. (3) and (4), and three different cones (NV_1: light green, NV_2: light yellow, NV_3: nattier blue) around the magnetic field vector that are the possible orientations of NV_1 axis, NV_2 axis and NV_3 axis as shown in Fig. 4(a). By using the Nelder–Mead algorithm for Eqs. (5) and (6), we can calculate the results $NV_0 = (2.03 \pm 0.20°, 287.48 \pm 23.04°)$ (red), $NV_1 = (110.81 \pm 0.48°, 331.57 \pm 0.44°)$ (green), $NV_2 = (107.69 \pm 0.27°, 91.30 \pm 0.80°)$ (yellow) and $NV_3 = (109.97 \pm 0.84°, 210.54 \pm 0.42°)$ (blue) shown in Fig. 4(b) and Table 1. In order to verify the accuracy of the results, the theoretical transition frequencies of the fourth kind of NV center (NV_0) are calculated as $NV_{0L}(\nu_1) = 2807.704$ MHz and $NV_{0R}(\nu_2) = 2941.211$ MHz by Eqs. (3) and (4). This formula $\nu = D_{gs}(1 \pm (\frac{\mu_B g_e B}{hD_{gs}} \cos\alpha) + \frac{3}{2}(\frac{\mu_B g_e B}{hD_{gs}})^2 \sin^2\alpha \pm (\frac{\mu_B g_e B}{hD_{gs}})^3(\frac{1}{8}\sin^3\alpha\tan\alpha - \frac{1}{2}\sin^2\alpha\cos\alpha)$. The experimental measured values of ν_1 and ν_2 for NV_0 are equal to 2806.54±0.16 MHz and 2942.22±0.16 MHz as shown in Table 1. We find that there are deviations of 1.16 MHz and 1.01 MHz with errors of 1.71% and 1.48%, respectively, between the theoretical and experimental results for left and right resonance peaks of NV_0 center. The deviation may come from strain of lattice and temperature fluctuation during measurement process.

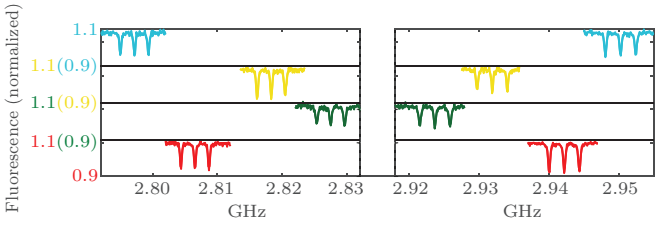


Fig. 3. ODMR spectra for NV centers in different orientations. In the static magnetic field, different NV centers have anisotropic Zeeman splitting and ODMR spectra. Because of hyperfine interaction with the electron spin and ^{14}N nuclear spin, the transitions between $m_s = 0$ and $m_s = \pm 1$ both have three peaks, respectively. These solid broken line and curve (red, green, yellow, and nattier blue) represent the experimental data and the data of fitting using Lorentzian functions for NV_i center ($i = 0, 1, 2, 3$).

In Table 1, the azimuth (ϕ) error of NV_0 is relatively large. The polar angle θ_{NV0} of NV_0 axis is close to zero, which almost coincides with the direction of the north pole. Around the north pole, the azimuth angle is completely uncertain. The orientation error of four kinds of NV centers are less than 0.93°.

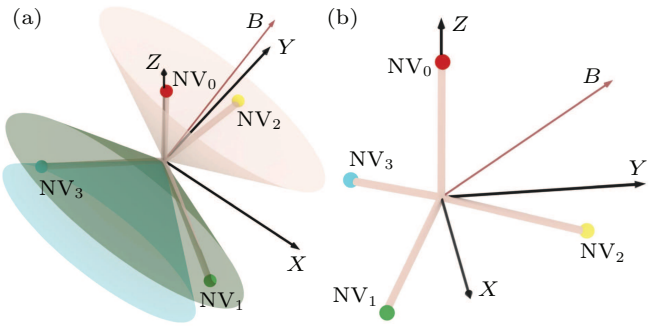


Fig. 4. (a) Possible orientation of the NV axis. The angles α between the magnetic field $\boldsymbol{B}$ and the NV_{1-3} axis are 116.64° (light green), 58.15° (light yellow), and 135.44° (nattier blue), respectively, showing that the possible NV axis is a cone around the magnetic field vector. (b) Four orientation of NV axis calculated with the Nelder–Mead algorithm. The calculated NV axis results are $NV_0 = (2.03 \pm 0.20°, 287.48 \pm 23.04°)$ (red), $NV_1 = (110.81 \pm 0.48°, 331.57 \pm 0.44°)$ (green), $NV_2 = (107.69 \pm 0.27°, 91.30 \pm 0.80°)$ (yellow) and $NV_3 = (109.97 \pm 0.84°, 210.54 \pm 0.42°)$ (blue).

3. Conclusions

In summary, we propose and demonstrate an efficient method to simultaneously identify four types of NV axis information with a direction-known magnetic field in a bulk diamond. Our method only needs to measure a set of ODMR spectra and then extract the polar angle of each NV center and magnetic field. Combining with the polar angle information of different NV centers, we finally employ the Nelder–Mead algorithm to calculate the orientation information of NV axis. Our method is fast and effectively to determine the orientation of the NV axis for ensembles and single spins in single crystal samples. This method can be directly extended to the orientation determination of NV centers in a micro-diamond, and easily applied in quantum sensing of vector magnetic and electric fields in the future.

Acknowledgements

This work was supported by the National Key R&D Program of China (Grant No. 2020YFA0309400), the National Natural Science Foundation of China (Grant No. 12174081), and the Fundamental Research Funds for the Central Universities (Grant Nos. JZ2021HGTB0126 and PA2021KCPY0052).

References

[1] Degen C L, Reinhard F and Cappellaro P 2017 *Rev. Mod. Phys.* **89** 035002
[2] Doherty M W, Manson N B, Delaney P, *et al.* 2013 *Phys. Rep.* **528** 1
[3] Van der Sar T, Wang Z, Blok M, Bernien H, Taminiau T, Toyli D, Lidar D, Awschalom D, Hanson R and Dobrovitski V 2012 *Nature* **484** 82
[4] Shi F, Zhang Q, Wang P, *et al.* 2015 *Science* **347** 1135
[5] Neumann P, Jakobi I, Dolde F, *et al.* 2013 *Nano Lett.* **13** 2738
[6] Balasubramanian G, Chan I Y and Kolesov R 2008 *Nature* **455** 64
[7] Liu G Q, Xing J and Pan X Y 2018 *Acta Phys. Sin.* **67** 120302 (in Chinese)
[8] Bar-Gill N, Pham L M, Jarmola A, *et al.* 2013 *Nat. Commun.* **4** 1743
[9] Gruber A, Drabenstedt A, Tietz C, Fleury L, Wrachtrup J and Borczyskowski C V 1997 *Science* **276** 2012
[10] Tusun M, Rong X and Du J 2019 *Chin. Phys. B* **28** 024204
[11] Iwasaki T, Naruki W, Tahara K, *et al.* 2017 *ACS Nano* **11** 1238
[12] Dolde F, Fedder H, Doherty M W, *et al.* 2011 *Nature Phys.* **7** 459
[13] Maertz B, Wijnheijmer A, Fuchs G, Nowakowski M and Awschalom D 2010 *Appl. Phys. Lett.* **96** 092504
[14] Rondin L, Tetienne J P, Rohart S, *et al.* 2013 *Nat. Commun.* **4** 2279
[15] Chen B, Hou X, Ge F, Zhang X, Ji Y, Li H, Qian P, Wang Y, Xu N and Du J 2020 *Nano Lett.* **20** 8267
[16] Ye J F, Jiao Z, Ma K, Huang Z Y, Lv H J and Jiang F J 2019 *Chin. Phys. B* **28** 047601
[17] Doherty M W, Acosta V M, Jarmola A, Barson M S, Manson N B, Budker D and Hollenberg L C 2014 *Phys. Rev. B* **90** 041201
[18] Delord T, Nicolas L, Bodini M and Hétet G 2017 *Appl. Phys. Lett.* **111** 013101
[19] Ho K O, Leung M Y, Jiang Y, Ao K P, Zhang W, Yip K Y, Pang Y Y, Wong K C, Goh S K and Yang S 2020 *Phys. Rev. Appl.* **13** 024041
[20] Hsieh S, Bhattacharyya P, Zu C, Mittiga T, Smart T, Machado F, Kobrin B, Höhn T, Rui N, Kamrani M, *et al.* 2019 *Science* **366** 1349
[21] Pham L M, Bar-Gill N, Le Sage D, Belthangady C, Stacey A, Markham M, Twitchen D, Lukin M D and Walsworth R L 2012 *Phys. Rev. B* **86** 121202
[22] Lai N D, Zheng D, Treussart F and Roch J F 2010 *Adv. Nat. Sci: Nanosci. Nanotechnol.* **1** 015014
[23] Fukushige K, Kawaguchi H, Shimazaki K, Tashima T, Takashima H and Takeuchi S 2020 *Appl. Phys. Lett.* **116** 264002
[24] Schloss J M, Barry J F, Turner M J and Walsworth R L 2018 *Phys. Rev. Appl.* **10** 034044
[25] Neumann P 2012 *Towards a room temperature solid state quantum processor—the nitrogen-vacancy center in diamond* Ph.D. Dissertation (University of Stuttgart, Germany)
[26] Barry J F, Schloss J M, Bauch E, Turner M J, Hart C A, Pham L M and Walsworth R L 2020 *Rev. Mod. Phys.* **92** 015004
[27] Milligan T 1999 *IEEE Trans. Antennas Propag.* **41** 78